Sitewise manipulations and Mott insulator-superfluid transition of interacting photons using superconducting circuit simulators

Xiuhao Deng,[1] Chunjing Jia,[2,3] and Chih-Chun Chien[1,*]
[1]*School of Natural Sciences, University of California, Merced, California 95343, USA*
[2]*Department of Applied Physics, Stanford University, Stanford, California 94305, USA*
[3]*Stanford Institute for Materials and Energy Sciences, SLAC National Accelerator Laboratory, 2575 Sand Hill Road, Menlo Park, California 94025, USA*

(Received 30 October 2014; revised manuscript received 13 January 2015; published 23 February 2015)

The Bose-Hubbard model (BHM) of interacting bosons in a lattice has been a paradigm in many-body physics, and it exhibits a Mott insulator-superfluid (MI-SF) transition at integer filling. Here a quantum simulator of the BHM using a superconducting circuit is proposed. Specifically, a superconducting transmission line resonator supporting microwave photons is coupled to a charge qubit to form one site of the BHM, and adjacent sites are connected by a tunable coupler. To obtain a mapping from the superconducting circuit to the BHM, we focus on the dispersive regime where the excitations remain photonlike. Standard perturbation theory is implemented to locate the parameter range where the MI-SF transition may be simulated. This simulator allows single-site manipulations, and we illustrate this feature by considering two scenarios where a single-site manipulation can drive a MI-SF transition. The transition can be analyzed by mean-field analyses, and the exact diagonalization was implemented to provide accurate results. The variance of the photon density and the fidelity metric clearly show signatures of the transition. Experimental realizations and other possible applications of this simulator are also discussed.

DOI: 10.1103/PhysRevB.91.054515 PACS number(s): 42.50.Pq, 05.30.Jp, 74.81.Fa, 02.70.−c

I. INTRODUCTION

Intensive research has been focused on simulating complex matter using well-controlled quantum systems in order to better understand their behavior and create useful analogs [1–6]. Successful examples include cold atoms trapped in optical potentials [2], trapped ions [1,4], spins in defects in diamonds [5], photonic arrays [3], etc. Recently, another class of quantum simulators based on superconducting circuits has opened more opportunities [7–11], which are made possible due to progress in fabricating well-designed circuits on chips. In those superconducting circuits, dissipation and decoherence have been suppressed significantly [9,12]. Moreover, interacting superconducting qubits and resonators can be fabricated on a chip, where quantum error-correction encoding and high-fidelity operations have been realized [13,14]. Various designs of couplers for connecting different qubits or resonators with wide tuning ranges have also been demonstrated [15–17]. The progress in superconducting circuits provides a promising perspective of scalable superconducting circuits as quantum simulators for many-body systems, which may be bosonic [7,18–20] or fermionic [21,22] in nature.

The Bose-Hubbard model (BHM) has been a paradigm in many-body theories, and the Mott insulator-superfluid (MI-SF) phase transition associated with the BHM has been of broad interest [2,23]. This transition was observed unambiguously in cold atoms trapped in optical lattices and can be probed with single-atom resolutions [24–26]. On the other hand, a theoretical framework for obtaining the BHM using the Jaynes-Cummings Hubbard model has been established [27,28]. Simulating this general model in cavity arrays has been proposed [27,29–31]. One may envision that introducing inhomogeneity into the BHM parameters can lead to richer physics, some of which has been explored in Refs. [32,33]. Simulating those phenomena requires tunability of single-site parameters, which could be hard in currently available simulators [1,2,4–6].

As a candidate for quantum simulators, a superconducting circuit has the following additional features [6,7,34]: (i) The circuit can be manipulated by applying voltages, currents, and/or magnetic flux. Hence useful classical circuit techniques can be introduced in similar ways. (ii) Circuit manipulations can be implemented locally to a single site/unit or globally to the whole system. (iii) The circuit can be tailored to a certain characteristic frequency, interaction strength, etc., and the circuit geometry can be fabricated in desired patterns. Furthermore, according to recent reports, the decoherence time of superconducting qubits based on different superconducting circuits approaches 0.1 ms [35–38]. The Q factor of an on-chip transmission line resonator [39] can even go beyond 10^5. A three-dimensional (3D) superconducting resonator [12,36] can have a quality factor up to 10^9, which implies that the lifetime of photons in superconducting resonators may approach 10 ms. This is good enough to allow one to practically consider the photon number as a conserved quantity in the circuit if the photon lifetime is compared to the operation frequency in the circuit typically in the range of 100 MHz to 10 GHz [9,34,40,41].

Having those features of superconducting circuit in mind, we propose a scheme to simulate the BHM with controllable inhomogeneous parameters. To demonstrate some interesting features, we consider how the phase transition between the delocalized SF and localized Mott insulator can be induced by manipulating the parameters of one single site. In conventional setups, global parameters such as the overall density or interaction drive the system across this transition, and here

*cchien5@ucmerced.edu

we propose that in superconducting-circuit simulators, one may observe this transition with a single-site manipulation by exploiting the sensitivity to the commensurate filling close to the transition. The details of our proposed scheme are verified by the exact diagonalization method [42], which already shows signatures of this transition in moderate-size systems. Thus this proposed scheme should be feasible in experiments.

Here the simulator is based on an array of superconducting transmission line resonators (TLRs). The goal is to simulate the BHM [23],

$$H = -\sum_i \mu_i n_i + \sum_i \frac{U_i}{2} n_i(n_i - 1) - \sum_i t_i (b_i^\dagger b_{i+1} + b_i b_{i+1}^\dagger). \quad (1)$$

Here μ_i is the on-site energy and plays the role of the chemical potential, U_i is the on-site interaction, and t_i is the nearest-neighbor hopping coefficient. In cold atoms one can control the filling and motion of a single atom [24], but manipulations of the energy and interaction on each site remain a challenge.

A superconducting TLR with a length in the range of centimeters can support a microwave resonant frequency corresponding to the oscillations of the electric potential and magnetic flux from the standing waves of the Cooper-pair density. Those microwaves are referred to as the photons in the TLR [43]. The quantum electrodynamics (QED) framework can then be applied to the TLR-qubit system to get the so-called circuit QED [43]. A single site of the system is modeled by the Jaynes-Cummings (JC) model [44], while an array of circuit QED systems, as schematically shown in Fig. 1, can be described by the Jaynes-Cummings Hubbard model [45],

$$H = \sum_n \left[\hbar\omega_n^c a_n^\dagger a_n + \hbar\omega^q \sigma_n^z + g_n(a_n\sigma_n^+ + a_n^\dagger\sigma_n^-)\right] + \sum_n J_n (a_n^\dagger a_{n+1} + a_n a_{n+1}^\dagger), \quad (2)$$

where ω_n^c is the cavity frequency, ω^q is the qubit frequency, g_n is the coupling strength between the cavity and qubit, and J_n is the effective hopping coefficient between cavities.

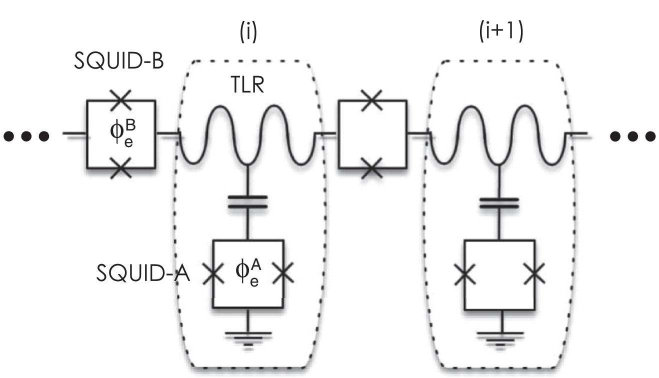

FIG. 1. Schematic plot of the 1D TLR array. SQUID A, as a tunable charge qubit, is capacitively coupled to the center of a TLR. Nearest-neighbor sites are connected by SQUID B. The external magnetic fluxes ϕ_e^A and ϕ_e^B through SQUIDS A and B can be used to tune their Josephson energies.

When the qubit is close to resonance with the cavity, they are coexcited, and the excitation on a single site has the form of a polariton. Simulating polaritonic many-body behavior has been studied recently based on various physical systems [19,46,47]. Here we consider a different regime in the parameter space to take advantage of the tunability of superconducting quantum circuits. We focus on the dispersive regime [27], where the excitation is limited in the TLR, while the qubit stays in its ground state. Hence the on-site excitation becomes photonic. In this regime, a perturbation calculation shows that the system can simulate the BHM. To make connections to experiments, feasible controlling and probing methods of the quantum phase transition between localized and delocalized states will be discussed. The exact diagonalization (ED) [42] method is used to numerically demonstrate the details of the phase transition.

II. ARCHITECTURE OF THE SIMULATOR

As illustrated in Fig. 1, the proposed simulator is a one-dimensional (1D) array of superconducting circuit elements. One site is formed by a TLR capacitively coupled to a superconducting charge qubit [9,34,40,41], which is labeled as SQUID A, and the qubit energy is tunable. The TLRs on different sites are connected via SQUID B, which leads to tunable couplings between nearest-neighbor sites. Here a derivation of how the Bose-Hubbard Hamiltonian (1) can be simulated by the superconducting circuit will be presented. Here we will use Hz $\times$ 2π as the unit of energy and set $\hbar \equiv 1$.

A. TLR as a lattice element

The qubit-TLR system is an analog of an atom-cavity system. In the strong-coupling regime the dynamics of the latter system can be modeled by the Jaynes-Cummings Hamiltonian [43]. Our superconducting circuit Hamiltonian can be derived following the work of circuit QED in Refs. [43,48,49]. The Hamiltonian of a single lattice site is

$$H^{\text{site}} = H^{\text{TLR}} + H^{\text{qubit}}. \quad (3)$$

The TLR with length D could be treated as a cavity with a single mode of the first harmonic. The excitation in the TLR is modeled as

$$H^{\text{TLR}} = \omega^c a^\dagger a. \quad (4)$$

The cavity frequency is $\omega^c = \frac{2\pi}{\sqrt{C^c L^c}} = 2\pi\sqrt{E_c^c E_L^c}$, where the net capacitance and inductance of the TLR are C^c and L^c, and the charge and inductive energies of the cavity are $E_c^c = \frac{(2e)^2}{C^c}$ and $E_L^c = \frac{1}{L^c(2e)^2}$. For the first harmonic, the spatial distribution [43] of N peaks at $x = -\frac{D}{2}, 0, \frac{D}{2}$. The node charge number and node flux at the maxima correspond to $N = \sqrt{\omega^c/E_c^c}(a^\dagger + a)$ and $\phi^c = -i\sqrt{\omega^c/E_L^c}(a^\dagger - a)$.

Since the qubit consists of two Josephson junctions in a superconducting loop, its Hamiltonian is

$$H^{\text{qubit}} = E_c^A(n - n_g)^2 - 2E_J^A \cos\left(\frac{\phi_e^A}{2}\right)\cos\phi. \quad (5)$$

Here $n = C_\Sigma^A V_J/2e$ and $n_g = C_g^A V_g/2e$ are the numbers of Cooper pairs on the island and the gate, respectively.

The capacitance between the qubit and TLR is C_g^A. $E_c^A = \frac{(2e)^2}{2C_\Sigma^A}$, with C_Σ^A being the total effective capacitance in the qubit. The Josephson tunneling energy is E_J^A, and the phase ϕ displaces the number of Cooper pairs. Because of the giant Kerr effect due to the Josephson junction, the energy difference between the lowest two levels $|0\rangle$ and $|1\rangle$ is separated from the other energies. Therefore SQUID A in Fig. 1 behaves like a superconducting qubit [34] with the Hamiltonian $H^{\text{qubit}} = -E_c^A \frac{1-2n_g}{2}\widetilde{\sigma}^z - E_J^A \cos(\frac{\phi_e^A}{2})\widetilde{\sigma}^x$, where $\widetilde{\sigma}^x = |0\rangle\langle 1| + |1\rangle\langle 0|$ and $\widetilde{\sigma}^z = -|0\rangle\langle 0| + |1\rangle\langle 1|$. Furthermore, $n_g = n^{dc} + C_g^A\sqrt{\omega^c/E_c^c}(a^\dagger + a)$ by investigating the gate voltage V_g at the point of the TLR to which the qubit couples, which includes the dc gate voltage on the qubit and a quantum mode of the TLR: $V_g = V^{dc} + \widehat{V^{ac}}$. As Fig. 1 shows, the qubit is coupled to the center of the TLR, so $\widehat{V^{ac}} = \sqrt{2}eN/C^c = \sqrt{\omega^c/2C^c}(a^\dagger + a)$ for the fundamental mode.

Here we focus on the case when the dc gate voltage bias is at the degeneracy point, $n^{dc} = \frac{1}{2}$. Then by introducing $|\uparrow\rangle = (|0\rangle + |1\rangle)/\sqrt{2}$ and $|\downarrow\rangle = (|0\rangle - |1\rangle)/\sqrt{2}$ with $\sigma^x = |\uparrow\rangle\langle\downarrow| + |\downarrow\rangle\langle\uparrow|$ and $\sigma^z = -|\downarrow\rangle\langle\downarrow| + |\uparrow\rangle\langle\uparrow|$ and dropping constant terms, the one-site Hamiltonian becomes

$$H^{\text{site}} = \omega^c a^\dagger a + \frac{\omega^q \sigma^z}{2} + g^q \sigma^x (a^\dagger + a), \tag{6}$$

where $\omega^q = 2E_J^A \cos(\frac{\phi_e^A}{2})$ and $g^q = 2e\frac{C_g^A}{C_\Sigma^A}\sqrt{\omega^c C^c}$. We define $H_0 = \omega^c(a^\dagger a - \sigma^z/2)$ and $V = \Delta\sigma_z/2 + g^q\sigma^x(a^\dagger + a)$, with $\Delta = \omega^c - \omega^q$ being the detuning between the cavity and qubit frequencies. Thus $H^{\text{site}} = H_0 + V$, and V is treated as a perturbation.

The qubit frequency and cavity frequency are in the same range of about 10 GHz, so it is natural to apply the rotating-wave approximation (RWA). Then $\Delta \ll \omega^c + \omega^q$. Moving into the interaction picture and rotating frame, one gets the Jaynes-Cummings interaction $g^q(\sigma_+ e^{i\omega^q t} + \sigma_- e^{-i\omega^q t})(a^\dagger e^{i\omega^c t} + ae^{-i\omega^c t}) \overset{\text{RWA}}{\approx} g^q(\sigma_- a^\dagger e^{i\Delta t} + \sigma_+ a e^{-i\Delta t})$, where $\sigma_\pm$ are the ladder operators. Moving back to the nonrotating frame, we get an effective interaction $g^q(\sigma^- a^\dagger + \sigma^+ a)$. Here we consider the dispersive regime [28,50,51], so $\Delta \gg g^q$ and there is virtually no excitation from $|\uparrow\rangle$ to $|\downarrow\rangle$. Applying standard perturbation theory with $E_\uparrow^{(0)} = 0$, $E_\downarrow^{(0)} = \Delta$, $V_{\uparrow\uparrow} = V_{\downarrow\downarrow} = 0$, $V_{\uparrow\downarrow} = g^q a^\dagger = V_{\uparrow\downarrow}^\dagger$ and going up to the fourth order, the quartic Kerr term gives rise to an effective on-site interaction.

Going back to the Schrodinger picture, the single-site Hamiltonian becomes

$$H^{\text{site}} = \omega^{c,\text{eff}} a^\dagger a + \frac{\omega^q}{2}\sigma^z + \left(\frac{g^q}{\Delta}\right)^3 g^q a^\dagger a(a^\dagger a - 1). \tag{7}$$

The charge qubit could be either a single Cooper-pair transistor or a transmon [34,40,41,52] whose qubit frequency can be tuned by changing the magnetic flux bias through a SQUID loop in the qubit circuit. $\omega^{c,\text{eff}} = \omega^c - \frac{g^{q2}}{\Delta} + (\frac{g^q}{\Delta})^3 g^q$ is the effective on-site frequency, and the quartic term is the effective on-site interaction of the photons. Those two terms are functions of the controllable parameter Δ. Assuming $g^q = 120\text{ MHz} \times 2\pi$ [9,41], $\Delta \geqslant 0.9\text{ GHz} \times 2\pi$, so $(\omega^c - \omega^{c,\text{eff}}) \in [-0.1,0.1]\text{ GHz} \times 2\pi$. We remark that the case $\Delta \sim g^q$, where the excitations are polaritons rather than photons, has been discussed in the literature [46].

B. Tunable TLR array

Different architectures for implementing a tunable coupler between two superconducting TLRs have been realized and discussed in Refs. [16,17,53–56]. Here we present a basic design. As shown in Fig. 1, SQUID B, with size and energy different from those of SQUID A, is coupled to adjacent TLRs. The coupling Hamiltonian is

$$H^B = \sum_{i=\text{upp,low}} \left[\frac{C_J^B}{2}\left(\dot{\phi}_i^{jj}\right)^2 + E_J^B\left(1 - \cos\phi_i^{jj}\right)\right], \tag{8}$$

where $\phi_{i=\text{upp,low}}^{jj}$ are the phase differences across the upper and lower Josephson junctions of SQUID B (see Fig. 1). The two Josephson junctions in SQUID B are assumed to be uniform with the same capacitance C_J^B and Josephson energy E_J^B. The external magnetic flux bias through SQUID B is $\phi_e^B = \phi_{\text{upp}}^{jj} + \phi_{\text{low}}^{jj}$ and $\dot{\phi}_{\text{upp}}^{jj} + \dot{\phi}_{\text{low}}^{jj} = \dot{\phi}_e^B = 0$. Here we introduce $\phi_{1,2}^c$ on the two ends connecting to TLRs 1 and 2 as the node phases and $N_{1,2}$ as the numbers of Cooper pairs on the node. According to the geometry of the SQUIDs, $\phi_1^c - \phi_2^c = \frac{1}{2}(\phi_{\text{upp}}^{jj} - \phi_{\text{low}}^{jj})$. Josephson equations then give $\frac{C_J^B}{2}(\dot{\phi}_{1,2}^c)^2 = \frac{1}{2}\frac{(2e)^2}{C_J^B}N_{1,2}^2 = E_c^B N_{1,2}^2$. Therefore the charge-energy term of H^B becomes $2E_c^B N_1^2 - 4E_c^B N_1 N_2 + 2E_c^B N_2^2$. Meanwhile, the Josephson energy is approximated by $E_J^B\cos(\frac{\phi_e^B}{2})[(\phi_1^c)^2 - 2\phi_1^c\phi_2^c + (\phi_2^c)^2]$, where higher-order terms are negligible because the phase difference across SQUID B $(\phi_{\text{upp}}^{jj} - \phi_{\text{low}}^{jj})$ can initially be set to zero by shorting both sides. It will be shown that $2E_J^B\cos(\frac{\phi_e^B}{2})$ can be tuned to the same order of magnitude as the on-site interaction term $(\frac{g^q}{\Delta})^3 g^q$ in Eq. (7), which is needed to place the system near the MI-SF phase transition.

The Hamiltonian for SQUID B, after those manipulations, becomes

$$H^B = \sum_{i=1,2}\left[2E_c^B N_i^2 + E_J^B\cos\left(\frac{\phi_e^B}{2}\right)\left(\phi_i^c\right)^2\right] - \left[4E_c^B N_1 N_2 + 2E_J^B\cos\left(\frac{\phi_e^B}{2}\right)\phi_1^c\phi_2^c\right]. \tag{9}$$

Here the simple harmonic terms inside the summation give an additional frequency shift to the TLR Hamiltonian in Eq. (4), which becomes $H_{\text{net},i}^{\text{TLR}} = \frac{1}{2}E_c^{c*}N_i^2 + \frac{1}{2}E_L^{c*}(\phi_i^c)^2$, with $E_c^{c*} = E_c^c + 4E_c^B$ and $E_L^{c*} = E_L^c + 2E_J^B\cos(\frac{\phi_e^B}{2})$. This corresponds to a dressed cavity frequency

$$\omega^{c*} = 2\pi\sqrt{E_c^{c*}E_L^{c*}} \tag{10}$$

as the TLRs are connected to an array with those SQUID Bs. The cross term in H^B leads to a coupling Hamiltonian $H^{\text{coup}} = -g^{\text{cap}}(a_1^\dagger + a_1)(a_2^\dagger + a_2) + g^{\text{ind}}(a_1^\dagger - a_1)(a_2^\dagger - a_2)$, with $g^{\text{cap}} = \omega^c E_c^B/E_c^{c*}$ and $g^{\text{ind}} = \omega^c 4E_J^B\cos(\frac{\phi_e^B}{2})/E_L^{c*}$. A similar coupling Hamiltonian can be found in Ref. [54], which is supported by experiments [15]. By considering two identical resonators $\omega_1^{c*} = \omega_2^{c*}$ and applying RWA and conservation of the photon number, one obtains

$$H_{12}^{\text{coup}} \simeq -(g^{\text{cap}} + g^{\text{ind}})(a_1^\dagger a_2 + a_1 a_2^\dagger). \tag{11}$$

We define $g = g^{\text{cap}} + g^{\text{ind}}$, which gives rise to the effective hopping J_n in Eq. (2).

For the simulator discussed here, typical values [9,41] of $E_c^B = 300$ MHz $\times 2\pi$, $E_J^B = 500$ MHz $\times 2\pi$, $E_c^{c*} = 10$ GHz $\times 2\pi$, $E_L^{c*} = 10$ GHz $\times 2\pi$ will be considered. Note that ϕ_e^B can be tuned within $[0,2\pi]$, so $g^{\text{ind}} \in [2,-2]$ GHz $\times 2\pi$. The net coupling strength is $g = -(g^{\text{cap}} + g^{\text{ind}}) \in [-2.3,1.7]$ GHz $\times 2\pi$. Since the perturbation approach is applied to the on-site Hamiltonian, in order to keep H^{coup} with the same order of magnitude as the highest-order term in Eq. (7), the coupling strength g has to fulfill the condition $g < g^q$. By biasing the system in the range ϕ_e^B around π, one should be able to get a smaller range of $g \in [-30,30]$ MHz $\times 2\pi$.

C. Superconducting-circuit simulator of the BHM

Collecting all terms, we obtain a many-body Jaynes-Cummings Hubbard Hamiltonian:

$$H^{\text{JCHM}} = \sum_i H_i^{\text{site}} + \sum_{\langle ij\rangle} H_{ij}^{\text{coup}}, \tag{12}$$

where $\langle ij\rangle$ denote nearest-neighbor pairs. In the dispersive regime, where our perturbation approach is applicable, the qubit does not get excitations and stays in its ground state. Therefore the qubit term $\sum_i \omega_i^q \sigma_i^z$ does not contribute to the many-body energy. In this case, the Jaynes-Cummings Hubbard model can be mapped to the Bose-Hubbard model [28] by treating the photons in the TLR as interacting bosons.

When compared to Eq. (1), the on-site energy, on-site interaction, and hopping terms are

$$\mu_i = -\left[\omega_i^{c*} - \left(\frac{g_i^q}{\Delta_i}\right) g_i^q + \left(\frac{g_i^q}{\Delta_i}\right)^3 g_i^q\right], \tag{13}$$

$$\frac{U_i}{2} = \left(\frac{g_i^q}{\Delta_i}\right)^3 g_i^q, \tag{14}$$

$$t_i = \left(g_i^{\text{cap}} + g_i^{\text{ind}}\right) = g_i. \tag{15}$$

As discussed previously, Δ_i and g_i can be tuned by a magnetic flux bias, so they are the independent variables in this model. One may recall that $|t| = |g| \in [0,30]$ MHz $\times 2\pi$ from previous discussions. In the dispersive regime $|\Delta| \in [0.35,1.0]$ GHz $\times 2\pi$ should give reasonable values [9,41] of $g^q = 120$ MHz $\times 2\pi$. Hence $U \in [0.0024,10]$ MHz $\times 2\pi$. To meet the traditional treatment of BHM, we analyze parameters in the unit of t. Thus $g^q/t \in [4,+\infty)$, $|\Delta/t| \in [10,+\infty)$, $U/t \in (0,+\infty)$, which implies that the range of U/t in this simulator should cover the MI-SF transition. To avoid going beyond the valid range of our approximation, the parameters are chosen in the range $|\Delta/t| \in [30,10^3]$.

In this simulation scheme the on-site energy μ_i, interaction strength U_i, and hopping coefficient t_i can be explicitly made site dependent, which leads to a versatile simulator of the BHM, especially if phenomena due to spatial inhomogeneity are of interest. When compared to ultracold atoms in optical lattices, this superconducting circuit simulator has some additional features. The interacting bosons in the simulator is confined inside the TLRs, so there is no need for background trapping potentials, which is common in cold-atom systems. Various geometries can be studied by fabricating the elements accordingly. In addition, open boundary conditions (OBCs) with hard walls can be introduced by terminating the coupling SQUID at the ends of the superconducting TLR array. Even in the presence of stray weak capacitive couplings, a high Q factor can still be maintained [39]. On the other hand, periodic boundary conditions (PBCs) can be realized by fabricating a loop structure so that bulk properties can be studied with a relatively small number of sites. The examples given in the following section will illustrate those features.

We remark that the wide range of U/t, which covers the SF-MI transition, is a consequence of the independent tunability of t and U in this simulator. Other interesting phenomena, such as the hard-core boson exhibiting nontrivial scaling behavior [57,58], may be beyond the scope of this simulator because t needs to remain finite as U goes to infinity. Such a regime requires $g^q/\Delta \to \infty$, so it is outside the dispersive regime investigated here.

III. SINGLE-SITE MANIPULATIONS OF THE MI-SF TRANSITION

Here we present one interesting application of this superconducting circuit simulator, where the MI-SF transition of the BHM can be induced by single-site manipulations. Other possible applications will be discussed later. To concentrate on the underlying physics, we consider a 1D array of N sites. The main idea is to exploit the commensurability of the BHM close to the MI-SF transition.

The parameters of a selected site (called site 1) are tuned by external magnetic flux through the charge qubit coupled to the TLR of this site. One may consider, for site 1, a shift of the on-site energy by δ and a shift of the on-site coupling constant by η. The choice of which site to manipulate is not important since the conclusions remain the same for the case with PBCs. According to Eq. (13), when the detuning energy between the qubit and TLR on site 1, Δ_1, is different from the detuning energy on the other sites $\Delta_i = \Delta_0, i = 2,\ldots,N$, the BHM parameters of site 1 are different from those on the other sites. Thus the BHM Hamiltonian of this 1D array with manipulations of site 1 is rewritten as

$$H = [\delta n_1 + \eta n_1(n_1-1)] - \mu\sum_{i=1}^{N} n_i + \frac{U}{2}\sum_{i=1}^{N} n_i(n_i-1) - t\sum_{i}^{N'}(b_i^\dagger b_{i+1} + b_{i+1}^\dagger b_i). \tag{16}$$

The first two terms summarize the effects of a different detuning on site 1. Here

$$\delta = -g_q^2\left(\frac{1}{\Delta_1} - \frac{1}{\Delta_0}\right) + g_q^4\left[\left(\frac{1}{\Delta_1}\right)^3 - \left(\frac{1}{\Delta_0}\right)^3\right],$$
$$\eta = g_q^4\left[\left(\frac{1}{\Delta_1}\right)^3 - \left(\frac{1}{\Delta_0}\right)^3\right]. \tag{17}$$

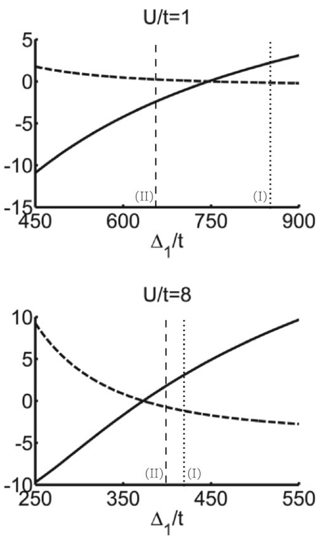

FIG. 2. δ (solid lines) and η (dashed lines) as functions of Δ_1 for $U/t = 1,5,8,10$ and $g_q = 120$ MHz $\times\, 2\pi$. As Eq. (16) shows, δ and η are the displacements of the on-site energy and on-site interaction of the first site. The vertical lines labeled (I) and (II) indicate the mean-field critical values of the two cases discussed in Sec. III.

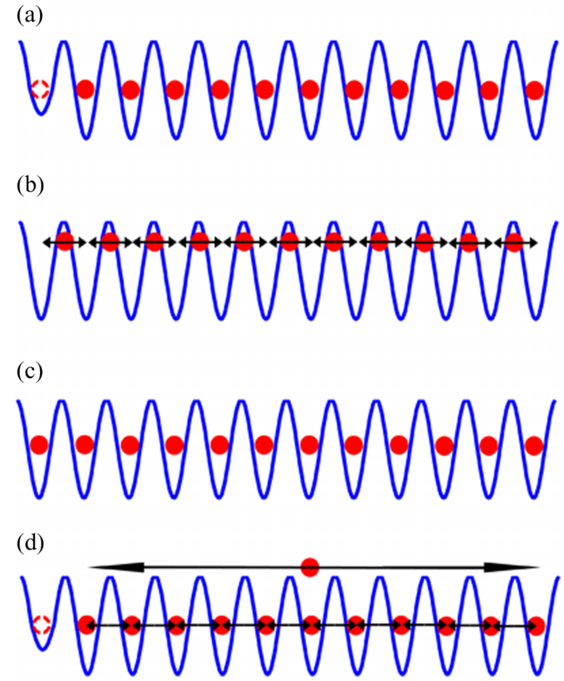

FIG. 3. (Color online) Illustration of single-site manipulations of the Mott insulator to superfluid transition (a) and (b) for $N-1$ bosons with strong repulsion in N sites and (c) and (d) for N bosons with strong repulsion in N sites. (a) The on-site energy of site 1 is increased, and the system is pushed into a localized Mott insulator. The dashed circle implies that the first site is virtually empty. (b) The system becomes a delocalized superfluid as the on-site energy is lowered. (c) The system is a localized Mott insulator when the on-site energy of site 1 is small. (d) By increasing the on-site energy of site 1, photons are pushed into the bulk and form a delocalized superfluid.

A diagram of δ and η as a function of Δ_1 is shown in Fig. 2, which gives an estimation of the BHM parameters in the presence of a single-site manipulation. $N' = N-1$ for the OBCs and $N' = N$ for the PBCs in the upper limit. We keep $t_i = t$ the same in the whole lattice because it does not depend on Δ_1. The unit of energy will be t. The value of U is fixed by Δ_0 and g_q.

We vary Δ_1/t as an independent variable. The advantages of this protocol are as follows: (1) The qubit energy is intact away from the manipulated site. (2) Particles are conserved in the whole system. We define the particle density ρ as the ratio between the photon number and site number. In the following we consider the phase transition due to this single-site manipulation when $\rho < 1$ and $\rho = 1$. For $\rho = (N-1)/N$ the system is a delocalized SF state in the absence of manipulations, and a single-site push leads to a localized MI state, which is shown schematically in Figs. 3(a) and 3(b). The second case with $\rho = 1$ is illustrated by Figs. 3(c) and 3(d), where the system is in an MI state without manipulations and becomes an SF after a single-site push.

To characterize those single-site manipulated transitions and to identify where the transitions take place, we analyze a useful quantity called the fidelity metric, which has been shown to capture quantum phase transitions or sharp quantum crossovers in the fermion Hubbard model [58,59] and other model Hamiltonians [60,61]. Given a Hamiltonian of the form $H(\lambda) = H_0 + \lambda H_1$, the fidelity is defined as the overlap between two (renormalized) ground states obtained with a small change $\delta\lambda$ in the parameter λ:

$$F(\lambda,\delta\lambda) = \langle \Phi_0(\lambda)|\Phi_0(\lambda+\delta\lambda)\rangle. \tag{18}$$

However, the fidelity has been shown to be an extensive quantity that scales with the system size [61,62]. Therefore the fidelity metric is introduced as [58,61,63]

$$g(\lambda,\delta\lambda) = (2/N)[1 - F(\lambda,\delta\lambda)]/\delta\lambda^2, \tag{19}$$

whose limit as $\delta\lambda \to 0$ is well defined away from the critical points and for which standard perturbation theories apply. More precisely,

$$\lim_{\delta\lambda\to 0} g(\lambda,\delta\lambda) = \frac{1}{N}\sum_{\alpha\neq 0} \frac{|\langle \Phi_\alpha(\lambda)|H_1|\Phi_0(\lambda)\rangle|^2}{[E_0(\lambda) - E_\alpha(\lambda)]^2}. \tag{20}$$

The fidelity metric measures how significantly the ground-state wave function changes as the parameter λ changes. A dramatic increase of the fidelity metric as a function of the varying parameter indicates a quantum phase transition or sharp quantum crossover [60].

A. Case 1: $\rho < 1$

When there are $(N-1)$ photons in an array of N sites, the ground state should be delocalized due to the incommensurate filling if all the sites have the same on-site energy and interaction energy. As will be shown in Figs. 4 and 5, nonuniform distributions of n_i and stronger fluctuations of the on-site photon density, quantified by the variance $\sigma_i = \langle\langle n_i^2\rangle - \langle n_i\rangle^2\rangle$, in the small Δ_1/t regime indicate delocalization of the photons with interactions up to $U = 10t$. By increasing the on-site energy of site 1, which can be performed by increasing Δ_1, a transition to a localized MI state of the remaining $N-1$ sites occurs. The setup is summarized in Figs. 3(a) and 3(b).

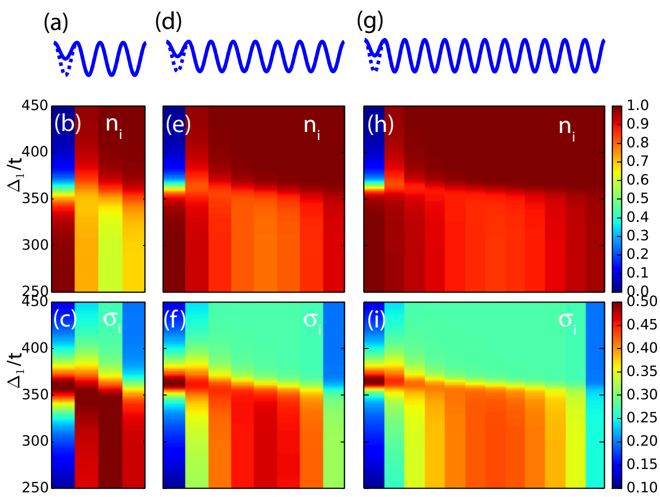

FIG. 4. (Color online) Exact diagonalization results of the density n_i and its variance σ_i as a function of Δ_1 for case 1 with OBCs. Sites 2 to N are uniform and $U = 10t$. (a)–(c) The results for a four-site array with three photons. In (a) the dashed line and solid line on the first site correspond to the two schemes shown in Fig. 3. (d)–(f) The case of eight sites with seven photons. (g)–(i) Twelve sites with 11 photons.

Based on current experimental technology [7,10,11,64], the size of the lattice in our exact diagonalization is chosen as $N = 4,8,12$. An estimation of the phase transition point can be obtained from a mean-field approximation.

For a homogeneous 1D array of N sites, the $(N-1)$ photons are not localized if the hopping coefficient is finite. By increasing the on-site energy of the first site, it becomes unfavorable if any particle hops into it. If the repulsive interactions between the bosons exceed the critical value of the MI-SF transition ($U_c/t \approx 3.28$ in 1D [65,66]), the ground state for the remaining $N-1$ sites becomes a Mott insulator with a wave function in Fock space as $|\varphi_1\rangle = |0,1,1,\ldots,1\rangle$. From the Hamiltonian (16), one gets the ground state energy $E_1 = \langle\varphi_1|H|\varphi_1\rangle = -\mu(N-1)$.

Then we estimate the ground state of a SF to determine where the transition occurs when Δ_1 is varied. In our mean-field approximation, a simplified trial ground state with no double (or higher) occupancy is used, which is appropriate for the case $U \gg t$. The trial ground state is $|\varphi_2\rangle = \frac{1}{\sqrt{N}}(|0,1,1,\ldots,1\rangle + |1,0,1,\ldots,1\rangle + |1,1,0,\ldots,1\rangle + \cdots + |1,1,1,\ldots,0\rangle)$. The ground-state energy is $E_2 = \langle\varphi_2|H|\varphi_2\rangle \approx \delta + \eta - 2t - \mu(N-1)$. The energy difference between the two ground states is

$$\Delta E = E_1 - E_2 \approx 2t - (\delta + \eta). \tag{21}$$

A phase transition occurs at the crossing point $\Delta E = 0$, or $(\delta + \eta) = 2t$. Thus the system forms a Mott insulator by emptying the first site. From Eqs. (17) and (21) we obtain an estimation of the phase-transition point at $\Delta_1 \approx 390t$ for $U = 10t$. The mean-field estimations are shown in Fig. 2. To check this prediction and provide more accurate estimations, we implement the ED method for several moderate-size systems. Figures 4 and 5 show ground-state properties, including n_i and σ_i on different sites as Δ_1 varies. The energy gap of the first excited state, shown in Fig. 6(a), verifies the existence of the SF (gapless) and MI (gapped) states.

The fidelity metric shown in Figs. 6(b) and 7 captures and locates the critical regime when the on-site energy of site 1 is manipulated. In Fig. 4, above $\Delta_1/t \approx 365$, the density is uniform away from site 1. The variance σ_i is also suppressed in the bulk. Thus the system is in the MI regime. Below $\Delta_1/t \approx 365$, the photons tend to congregate at the two ends of the array, but the variance is small. At the center of the array, the photon density is smaller, with a larger variance. This corresponds to a delocalized state. The density n_i thus captures the main conclusion of our mean-field analysis and shows corrections from finite-size effects.

The critical values in the numerical results are close to the mean-field estimations. The location of the critical point

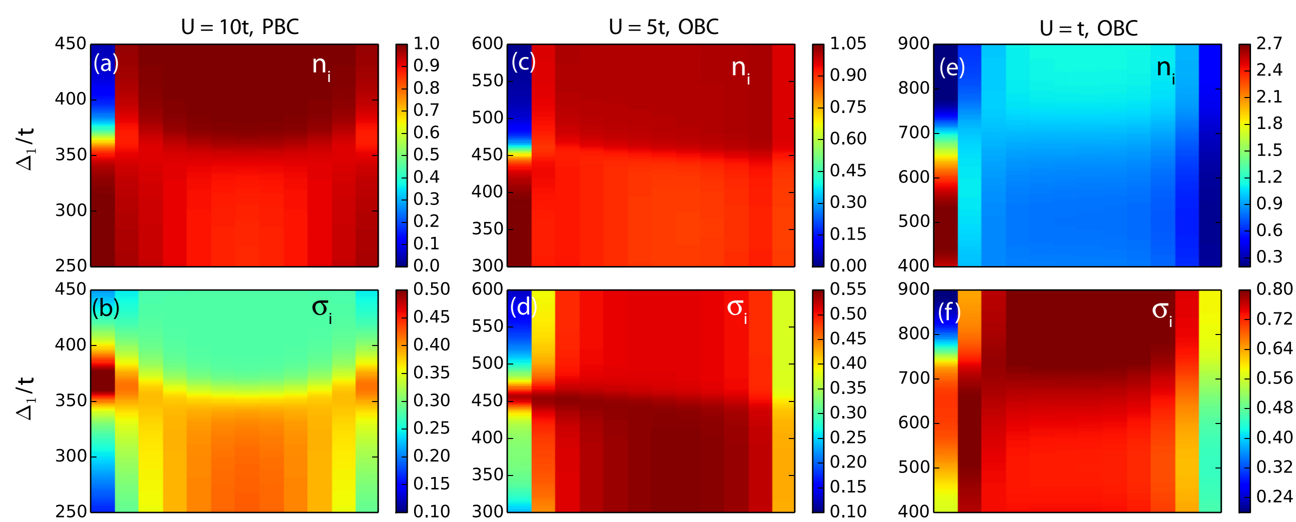

FIG. 5. (Color online) Photon density profiles and their variance for selected values of U and boundary conditions. (a) and (b): $U/t = 10$ and PBCs. In this case, the photons in sites 2 and N can both tunnel to site 1. Hence the photon densities on sites 2 and N are different from the bulk value due to boundary effects. (c) and (d): $U/t = 5$ and OBCs. (e) and (f): $U/t = 1$ and OBCs. The nonuniform density and its significant variance of the last case indicate that there is no Mott insulator in this setting. Here $N = 12$ with 11 photons.

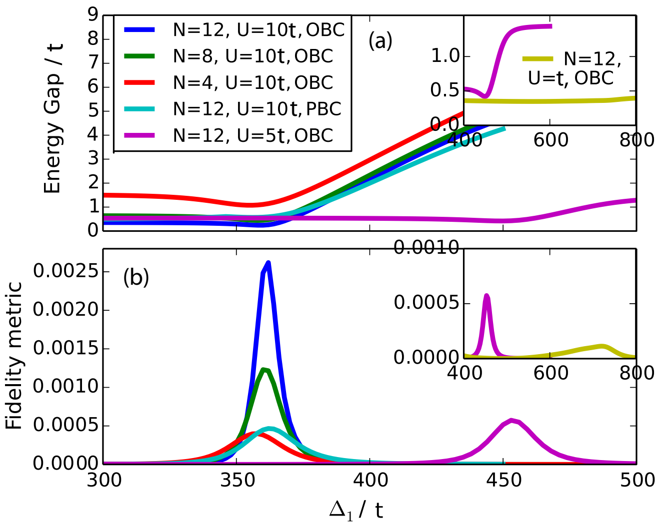

FIG. 6. (Color online) (a) Energy gap for different values of U and N. The inset shows a regime when $U=t$, in yellow, for $N=12$ with OBCs compared to $U=5t$ from the main figure. (b) The peaks of the fidelity metric indicate the critical points. When N varies, the location of the critical point remains intact. However, varying the on-site interaction U changes the location of the critical point, which is consistent with the analysis in Sec. III. Note that PBCs give the same critical point as OBCs.

does not change much as N changes, but the MI features become more prominent when N increases. Due to finite-size and boundary effects, the edge of the Mott insulator is distorted, but the bulk indeed exhibits features such as an integer filling and suppressed fluctuations σ_i. Boundary effects can also be observed on the neighbors of the manipulated site as their values of n_i deviate from the bulk. Those observations are also valid in Figs. 5(a) and 5(b), where site 1 is connected to site 2 and site 12 due to PBCs.

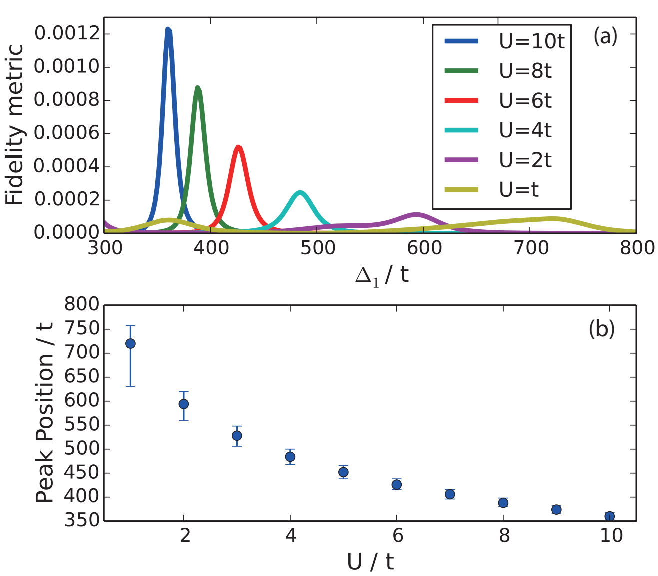

FIG. 7. (Color online) (a) Fidelity metric as a function of Δ_1 for different values of U for $N=8$ and 7 photons. (b) Peak position of the fidelity metric as a function of U/t. The full width at half maximum (FWHM) is shown as the bar spanning across each point.

For small U/t, as shown in Fig. 5(e), 5(f) and the insets in Fig. 6, the SF state dominates the whole parameter space explored in our ED calculations, which confirms that no artifact is induced if the system is in the SF regime. In the insets in Fig. 6, the results of a broader range of Δ_1 for the case of $U=t$ are shown, and the small, smooth gap throughout the range of Δ_1 is consistent with a SF state for the case $U=t$ in Figs. 5(e) and 5(f).

Figure 6 shows another signature of the phase transition as $\Delta_1/t \approx 365$ for $U=10t$ when $N=4$, 8, and 12, as indicated by a minimum in the energy gap followed by a rapid rise. For different values of U/t, Δ_i in the bulk are different according to Eq. (14). Hence the critical point shifts in the Δ_1/t axis according to Eqs. (17) and (21), and this is consistent with the results shown in Fig. 6.

B. Case 2: $\rho = 1$

As illustrated in Figs. 3(c) and 3(d), here we consider N photons placed in an N-site array. If U/t is large, the system is in a Mott insulator state. As the on-site energy of site 1 increases, the boson in that site is expected to be pushed to the bulk, and this should lead to a delocalized state because of the extra boson. Following a similar procedure, we estimate the critical value of Δ_1 that controls δ and η for this case.

The localized MI ground state can be written as $|\varphi_1\rangle = |1,1,1,\ldots,1\rangle$, with the ground-state energy $E_1 = \langle\varphi_1|H|\varphi_1\rangle = \delta - N\mu$. We consider a trial delocalized ground state $|\varphi_2\rangle = \frac{1}{\sqrt{N-1}}(|0,2,1,\ldots,1\rangle + |0,1,2,\ldots,1\rangle + \cdots + |0,1,1,\ldots,2\rangle)$, whose ground-state energy is $E_2 = \langle\varphi_2|H|\varphi_2\rangle \approx -N\mu + \frac{U}{2} - 2t$. Thus the energy difference is

$$\Delta E = E_1 - E_2 \approx \delta - \frac{U}{2} + 2t. \quad (22)$$

The MI-SF phase transition occurs when $\Delta E = 0$, and one may notice that the critical point depends explicitly on U, which is in contrast to the U-independent critical point in the mean-field analysis of case 1. For case 2 we find that the critical points are $\delta = 3t, \Delta_1 \approx 390t$ for $U/t = 10$ and $\delta = 0.5t, \Delta_1 \approx 445t$ for $U/t = 5$. The mean-field predictions are also shown in Fig. 2.

Numerical results from the ED method for this case are shown in Fig. 8. As shown in Figs. 8(a) and 8(b), below the critical point $\Delta_1 \sim 470t$, the system is an MI with one photon per site, and above $\Delta_1 \sim 470t$ the system becomes an SF with significant σ_i in the bulk. The fidelity metric shown in Fig. 8(d) verifies that the critical point is close to the estimation from our mean-field analysis. These results verify the feasibility of inducing and observing those transitions in moderate-sized systems.

IV. IMPLICATIONS FOR EXPERIMENTAL REALIZATION

State preparation. In the MI regime, the particle density on each site is an integer. One may prepare an arbitrary n-photon state in each site, including $n = 0,1$, that is of interest by adiabatically swapping the qubit state to the TLR [67,68]. This single-site preparation can be performed simultaneously on all the sites. Then starting from the MI regime, one can transform it to the many-body ground state for different cases.

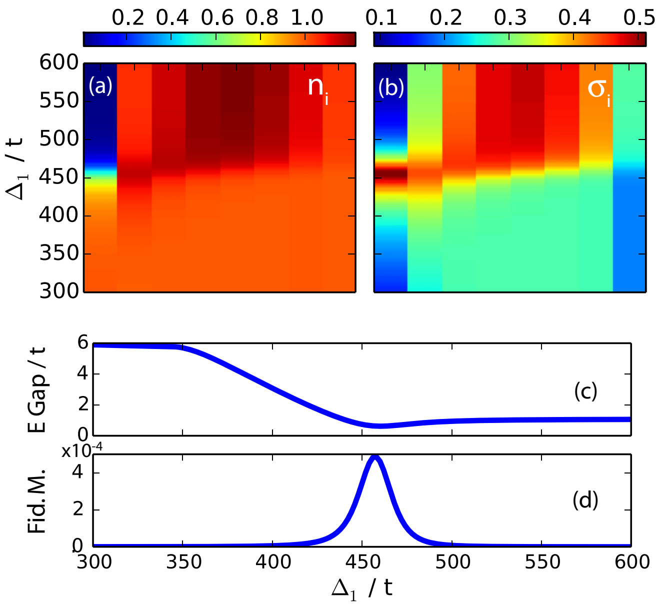

FIG. 8. (Color online) Exact diagonalization results for case 2 with $N = 8$ and eight photons. Here $U = 10t$. (a) The density profile in the array and (b) the density variance. (c) The energy gap (E Gap) and (d) fidelity metric (Fid. M.) clearly exhibit signatures of the MI-SF transition.

For example, in case 1 in Sec. III, the ground state in the MI regime is $|0,1,1,1,\ldots\rangle$. Recent work also proposes a scheme of an N-photon state preparation in a superconducting TLR array supported by numerical results [47].

Cooling. Solid-state simulators based on superconducting circuits, including the one we propose here, contain many degrees of freedom, which not only provide great tunability but also introduce relatively strong couplings to external fields. To experimentally implement the simulator proposed here, cooling such a complex system can be a great challenge. We suggest the following three stages. In stage 1, the whole system is kept in the superconducting phase and thermal excitations in the superconducting circuits, and Josephson junctions should be suppressed [9,34,40,41,69]. They are also associated with the suppression of dissipation and decoherence. As mentioned in the Introduction, the lifetime of the photons at this stage is already much longer than the operation time of the superconducting circuit by a factor of about 10^7.

In stage 2, cooling of the TLR-qubit single-site system should be performed before connecting the whole array. This is associated with the state preparation of the TLR array, and a degree of freedom different from that of stage 1 needs to be dealt with. The quantum computation community has been making significant progress related to the cooling at this stage [69]. Inspired by ideas from optical systems, Sisyphus cooling, dynamic cooling, and sideband cooling of superconducting systems have successfully cooled a qubit to its ground state [70–73].

In stage 3, once a multisite array is connected by turning on the hopping between adjacent sites, the desired many-body Hamiltonian follows. In order to simulate and observe the quantum phase transition discussed here, one needs to constantly cool the system and keep the number of photons conserved during the operation. This is more challenging than cooling just a single site, especially if inhomogeneity of the on-site energies is present. Applying a bias or other manipulations can cause excitations as well and needs to be performed quasiadiabatically. Moreover, taking out the heat from the multisite system when operating near the critical regime leads to yet another issue. Advanced schemes to cool a single site have been available, while cooling a multisite array like the one studied here has not been reported so far. The development of such technologies is important for realizing the proposed simulator. Based on current ground-state preparations and state-manipulation technologies developed in coupled superconducting cavity systems [74,75], it is promising that photon-number-conserving cooling processes may be realized by scaling up the cooling methods for those coupled systems.

Detection of the phase transition. Since the single-site manipulations of the MI-SF transition exhibit strong signatures in the density distribution, we briefly discuss a direct measurement of the photon numbers and number fluctuations on each site. Interestingly, the measurement can be turned on and off when needed to minimize the coupling of the simulator to those external circuits. As shown in Fig. 9, each site can be coupled to a memory TLR via the additional circuit. The central SQUID C is used to switch the coupling between the on-site unit and the measurement unit [79] for controlling the memorizing window. This is possible by changing the

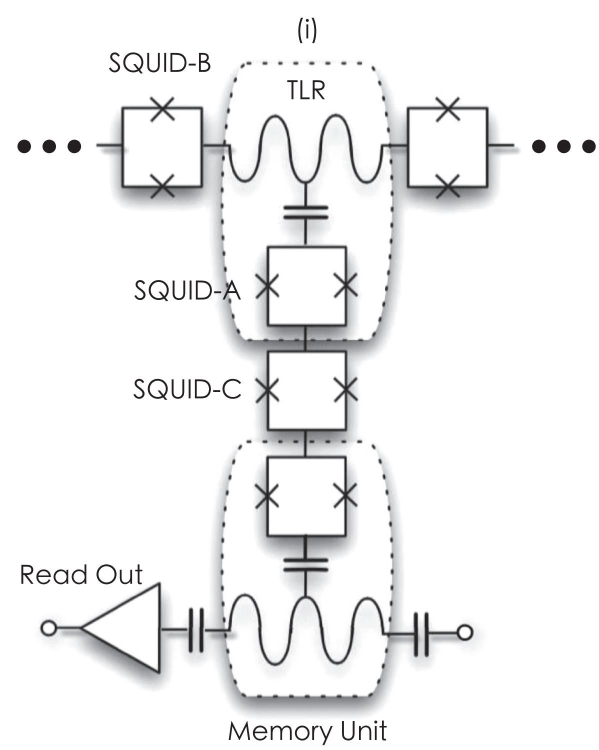

FIG. 9. Measuring the photons in the simulator: Each site of the simulator is connected to a memory unit formed by another qubit-TLR system via a tunable SQUID (labeled SQUID C) acting as a switch. Measurements of the photon number in the memory unit can be applied [76–78]. This memory unit can also serve as a circuit for preparing the initial state by manipulating SQUID C and SQUID B.

bias flux through SQUID C (labeled on Fig. 9), ϕ_m. A fast photon state SWAP between the two TLRs can be applied using a four-wave mixing scheme proposed in Ref. [50] to get $|n_{\text{on-site}} 0_{\text{measure}}\rangle \rightarrow |0_{\text{on-site}} n_{\text{measure}}\rangle$, so that the photons in the TLR of the simulator are transferred and stored in the measurement TLR. Fast measurements of single-photon states can be applied to measure photon numbers in the memory TLR with technologies recently developed in circuit QED [76–78,80–83]. By repeating the measurement one gets the average photon number $\langle n_i \rangle$ and variation $\langle \sigma_i \rangle$, as depicted in Fig. 4 for detecting different quantum phases in the TLR array.

The conservation of photon numbers is important in realizing the single-site induced MI-SF transitions. The circuit may lose or gain photons due to couplings to external circuits or the ac control signals in the circuit. Recent progress in superconducting quantum circuits has extended the lifetime of photons in each site with a TLR coupled to a qubit to milliseconds [12,36,39], which is long enough for practical photon-number conservation compared to the manipulations and measurements that are on the order of nanoseconds [9,34,40,41]. Furthermore, the couplers, SQUID B, can have energy scales very different from that of the photons in the simulator to avoid trapping photons. Therefore the photon numbers in the TLRs can be treated as constants. The manipulations, in particular those due to the couplers between sites, can be introduced in an adiabatic fashion and minimize photon loss. Even in driven systems a single photon can be transferred faithfully among multiple TLRs [74], which predicts a promising perspective for photon-conserving manipulations in quantum circuits. Other theoretical work [84–86] for number-conserving manipulations of photon excitations in superconducting circuits also provides exciting alternatives. Moreover, stabilizing photon coherent states in driven systems has been experimentally demonstrated [87]. This progress hints at the feasibility of the proposed simulator based on superconducting circuits.

V. CONCLUSION

A versatile quantum simulator of interacting bosons based on a tunable superconducting TLR-SQUID array has been presented. The BHM with tunable parameters on each site can be studied using the photons in this simulator. We have demonstrated the feasibility of inducing the MI-SF transition by manipulating only one single site. Our results are further supported by the exact diagonalization method, and details of the transition with realistic parameters are presented. The fidelity metric, energy gap, and on-site photon number show signatures of the phase transition. We also discussed possible schemes for state preparation, cooling, and detection of the phase transition for this proposed simulator.

Besides the manipulations of the phase transition discussed here, this quantum simulator is also capable of demonstrating topological properties in the BHM with superlattice structures and should exhibit the topological properties, edge states, and topological phase transitions studied in Refs. [32,33,88]. Moreover, quantum quenches [89,90] and their associated dynamics may also be simulated by this superconducting circuit simulator. For example, similar to Ref. [91], one can separate the TLR array into two sections by turning off the hopping between the two sections. Then different photon numbers are prepared in the two sections. By switching on the hopping between the two sections, photons are expected to slosh back and forth between the two sections, which should be detectable with similar measurement methods. Thus the superconducting circuit simulator adds more excitement to the physics of interacting bosons and complements other available simulators.

ACKNOWLEDGMENTS

We thank L. Tian and R. Chiao for valuable advice on this work and A. Sharybov, Y. Hu, K. Mitchell, and J. Sharping for useful discussions. The computations were performed using the resources of the National Energy Research Scientific Computing Center (NERSC) supported by the US Department of Energy, Office of Science, under Contract No. DE-AC02-05CH11231. Work at SLAC and Stanford University was supported by the U.S. Department of Energy, Office of Basic Energy Sciences, Division of Materials Science and Engineering, under Contract No. DE-AC02-76SF00515.

[1] R. Blatt and C. F. Roos, Nat. Phys. **8**, 277 (2012).
[2] I. Bloch, J. Dalibard, and S. Nascimbène, Nat. Phys. **8**, 267 (2012).
[3] A. Aspuru-Guzik and P. Walther, Nat. Phys. **8**, 285 (2012).
[4] P. Schindler, M. Müler, D. Nigg, J. T. Barreiro, E. A. Martinez, M. Hennrich, T. Monz, S. Diehl, P. Zoller, and R. Blatt, Nat. Phys. **9**, 361 (2013).
[5] J. Cai, A. Retzker, F. Jelezko, and M. B. Plenio, Nat. Phys. **9**, 168 (2013).
[6] I. M. Georgescu, S. Ashhab, and F. Nori, Rev. Mod. Phys. **86**, 153 (2014).
[7] A. A. Houck, H. E. Türeci, and J. Koch, Nat. Phys. **8**, 292 (2012).
[8] C. Bruder, R. Fazio, and G. Schön, Ann. Phys. (Leipzig) **14**, 566 (2005).
[9] M. H. Devoret and R. J. Schoelkopf, Science **339**, 1169 (2013).
[10] J. E. Mooij and G. Schön, Phys. B. (Amsterdam, Neth.) **152**, 212 (1988).
[11] R. Fazio and H. van der Zant, Phys. Rep. **355**, 235 (2001).
[12] M. Reagor, H. Paik, G. Catelani, L. Sun, C. Axline, E. Holland, I. M. Pop1, N. A. Masluk, T. Brecht, L. Frunzio, M. H. Devoret, L. Glazman, and R. J. Schoelkopf, Appl. Phys. Lett. **102**, 192604 (2013).
[13] R. Barends *et al.*, Nature (London) **508**, 500 (2014).
[14] J. M. Chow, J. M. Gambetta, E. Magesan, D. W. Abraham, A. W. Cross, B. R. Johnson, N. A. Masluk, C. A. Ryan, J. A. Smolin, S. J. Srinivasan, and M. Steffen, Nat. Commun. **5**, 4015 (2014).
[15] A. Baust, E. Hoffmann, M. Haeberlein, M. J. Schwarz, P. Eder, J. Goetz, F. Wulschner, E. Xie, L. Zhong, F. Quijandria, B. Peropadre, D. Zueco, J.-J. Garcia Ripoll, E. Solano, K. Fedorov, E. P. Menzel, F. Deppe, A. Marx, and R. Gross, Phys. Rev. B **91**, 014515 (2015).
[16] R. C. Bialczak, M. Ansmann, M. Hofheinz, M. Lenander, E. Lucero, M. Neeley, A. D. O'Connell, D. Sank, H. Wang,

M. Weides, J. Wenner, T. Yamamoto, A. N. Cleland, and J. M. Martinis, Phys. Rev. Lett. **106**, 060501 (2011).
[17] Y. Chen *et al.*, Phys. Rev. Lett. **113**, 220502 (2014).
[18] A. van Oudenaarden and J. E. Mooij, Phys. Rev. Lett. **76**, 4947 (1996).
[19] S. Schmidt and J. Koch, Ann. Phys. (Berlin) **525**, 395 (2013).
[20] M. Leib, F. Deppe, A. Marx, R. Gross, and M. J. Hartmann, New J. Phys. **14**, 075024 (2012).
[21] O. Viehmann, J. von Delft, and F. Marquardt, Phys. Rev. Lett. **110**, 030601 (2013).
[22] J. Q. You, Z. D. Wang, W. Zhang, and F. Nori, Sci. Rep. **4**, 5535 (2014).
[23] M. P. A. Fisher, P. B. Weichman, G. Grinstein, and D. S. Fisher, Phys. Rev. B **40**, 546 (1989).
[24] W. S. Bakr, J. I. Gillen, A. Peng, S. Fölling, and M. Greiner, Nature (London) **462**, 74 (2009).
[25] W. S. Bakr, A. Peng, M. E. Tai, R. Ma, J. Simon, J. I. Gillen, S. Fölling, L. Pollet, and M. Greiner, Science **329**, 547 (2010).
[26] D. Jaksch, C. Bruder, J. I. Cirac, C. W. Gardiner, and P. Zoller, Phys. Rev. Lett. **81**, 3108 (1998).
[27] M. J. Hartmann, F. Brandão, and M. Plenio, Laser Photonics Rev. **2**, 527 (2008).
[28] J. Koch and K. Le Hur, Phys. Rev. A **80**, 023811 (2009).
[29] A. D. Greentree, C. Tahan, J. H. Cole, and L. C. L. Hollenberg, Nat. Phys. **2**, 856 (2006).
[30] M. J. Hartmann and M. B. Plenio, Phys. Rev. Lett. **99**, 103601 (2007).
[31] M. J. Hartmann, F. G. S. L. Brand, and M. B. Plenio, Nat. Phys. **2**, 849 (2006).
[32] S.-L. Zhu, Z.-D. Wang, Y.-H. Chan, and L.-M. Duan, Phys. Rev. Lett. **110**, 075303 (2013).
[33] F. Grusdt, M. Höning, and M. Fleischhauer, Phys. Rev. Lett. **110**, 260405 (2013).
[34] Y. Makhlin, G. Schön, and A. Shnirman, Rev. Mod. Phys. **73**, 357 (2001).
[35] H. Paik, D. I. Schuster, L. S. Bishop, G. Kirchmair, G. Catelani, A. P. Sears, B. R. Johnson, M. J. Reagor, L. Frunzio, L. I. Glazman, S. M. Girvin, M. H. Devoret, and R. J. Schoelkopf, Phys. Rev. Lett. **107**, 240501 (2011).
[36] C. Rigetti, J. M. Gambetta, S. Poletto, B. L. T. Plourde, J. M. Chow, A. D. Córcoles, J. A. Smolin, S. T. Merkel, J. R. Rozen, G. A. Keefe, M. B. Rothwell, M. B. Ketchen, and M. Steffen, Phys. Rev. B **86**, 100506(R) (2012).
[37] Z. Kim, B. Suri, V. Zaretskey, S. Novikov, K. D. Osborn, A. Mizel, F. C. Wellstood, and B. S. Palmer, Phys. Rev. Lett. **106**, 120501 (2011).
[38] X.-H. Deng, Y. Hu, and L. Tian, Supercond. Sci. Technol. **26**, 114002 (2013).
[39] H. Wang, M. Hofheinz, J. Wenner, M. Ansmann, R. C. Bialczak, M. Lenander, E. Lucero, M. Neeley, A. D. O'Connell, D. Sank, M. Weides, A. N. Cleland, and J. M. Martinis, Appl. Phys. Lett. **95**, 233508 (2009).
[40] M. H. Devoret and J. M. Martinis, Quantum Inf. Process. **3**, 163 (2004).
[41] J. Clarke and F. K. Wilhelm, Nature (London) **453**, 1031 (2008).
[42] J.-M. Zhang and R.-X. Dong, Eur. J. Phys. **31**, 591 (2010).
[43] A. Blais, R.-S. Huang, A. Wallraff, S. M. Girvin, and R. J. Schoelkopf, Phys. Rev. A **69**, 062320 (2004).
[44] E. T. Jaynes and F. W. Cummings, Proc. IEEE **51**, 89 (1963).
[45] D. G. Angelakis, M. F. Santos, and S. Bose, Phys. Rev. A **76**, 031805 (2007).
[46] M. Leib and M. J. Hartmann, New J. Phys. **12**, 093031 (2010).
[47] K. Seo and L. Tian, arXiv:1408.2304.
[48] A. A. Houck, D. I. Schuster, J. M. Gambetta, J. A. Schreier, B. R. Johnson, J. M. Chow, L. Frunzio, J. Majer, M. H. Devoret, S. M. Girvin, and R. J. Schoelkopf, Nature (London) **449**, 328 (2007).
[49] L. S. Bishop, J. M. Chow, J. Koch, A. A. Houck, M. H. Devoret, E. Thuneberg, S. M. Girvin, and R. J. Schoelkopf, Nat. Phys. **5**, 105 (2009).
[50] A. V. Sharypov, X.-H. Deng, and L. Tian, Phys. Rev. B **86**, 014516 (2012).
[51] R. W. Boyd, *Nonlinear Optics*, 3rd ed. (Elsevier, Academic Press, Waltham, MA, USA, 2008).
[52] J. Koch, T. M. Yu, J. Gambetta, A. A. Houck, D. I. Schuster, J. Majer, A. Blais, M. H. Devoret, S. M. Girvin, and R. J. Schoelkopf, Phys. Rev. A **76**, 042319 (2007).
[53] J.-Q. Liao, J.-F. Huang, Y.-X. Liu, L.-M. Kuang, and C.-P. Sun, Phys. Rev. A **80**, 014301 (2009).
[54] B. Peropadre, D. Zueco, F. Wulschner, F. Deppe, A. Marx, R. Gross, and J. J. García-Ripoll, Phys. Rev. B **87**, 134504 (2013).
[55] R. A. Pinto, A. N. Korotkov, M. R. Geller, V. S. Shumeiko, and J. M. Martinis, Phys. Rev. B **82**, 104522 (2010).
[56] S. J. Srinivasan, A. J. Hoffman, J. M. Gambetta, and A. A. Houck, Phys. Rev. Lett. **106**, 083601 (2011).
[57] S. Sachdev, *Quantum Phase Transitions*, 2nd ed. (Cambridge University Press, Cambridge, 2011).
[58] L. Campos Venuti, M. Cozzini, P. Buonsante, F. Massel, N. Bray-Ali, and P. Zanardi, Phys. Rev. B **78**, 115410 (2008).
[59] C.-J. Jia, B. Moritz, C.-C. Chen, B. S. Shastry, and T. P. Devereaux, Phys. Rev. B **84**, 125113 (2011).
[60] M. Rigol, B. S. Shastry, and S. Haas, Phys. Rev. B **79**, 052502 (2009).
[61] L. Campos Venuti and P. Zanardi, Phys. Rev. Lett. **99**, 095701 (2007).
[62] W.-L. You, Y.-W. Li, and S.-J. Gu, Phys. Rev. E **76**, 022101 (2007).
[63] P. Zanardi and N. Paunkovic, Phys. Rev. E **74**, 031123 (2006).
[64] D. L. Underwood, W. E. Shanks, J. Koch, and A. A. Houck, Phys. Rev. A **86**, 023837 (2012).
[65] I. Danshita and A. Polkovnikov, Phys. Rev. A **84**, 063637 (2011).
[66] S. Ejima, H. Fehske, and F. Gebhard, Europhys. Lett. **93**, 30002 (2011).
[67] A. Wallraff, D. I. Schuster, A. Blais, L. Frunzio, R.-S. Huang, J. Majer, S. Kumar, S. M. Girvin, and R. J. Schoelkopf, Nature (London) **431**, 162 (2004).
[68] M. Hofheinz, H. Wang, M. Ansmann, R. C. Bialczak, E. Lucero, M. Neeley, A. D. O'Connell, D. Sank, J. Wenner, J. M. Martinis, and A. N. Cleland, Nature (London) **459**, 546 (2009).
[69] J. Q. You and F. Nori, Nature (London) **474**, 589 (2011).
[70] M. Grajcar, S. H. W. van der Ploeg, A. Izmalkov, E. Il'ichev, H.-G. Meyer, A. Fedorov, A. Shnirman, and G. Schön, Nat. Phys. **4**, 612 (2008).
[71] S. O. Valenzuela1, W. D. Oliver, D. M. Berns, K. K. Berggren, L. S. Levitov, and T. P. Orlando, Science **314**, 1589 (2006).
[72] J. Q. You, Y.-X. Liu, and F. Nori, Phys. Rev. Lett. **100**, 047001 (2008).

[73] N. Bergeal, R. Vijay, V. E. Manucharyan, I. Siddiqi, R. J. Schoelkopf, S. M. Girvin, and M. H. Devoret, Nat. Phys. **6**, 296 (2010).

[74] M. Mariantoni, H. Wang, R. C. Bialczak, M. Lenander, E. Lucero, M. Neeley, A. D. O'Connell, D. Sank, M. Weides, J. Wenner, T. Yamamoto, Y. Yin, J. Zhao, J. M. Martinis, and A. N. Cleland, Nat. Phys. **7**, 287 (2011).

[75] Y. Chen, P. Roushan, D. Sank, C. Neill, E. Lucero, M. Mariantoni, R. Barends, B. Chiaro, J. Kelly, A. Megrant, J. Y. Mutus, P. J. J. O'Malley, A. Vainsencher, J. Wenner, T. C. White, Y. Yin, A. N. Cleland, and J. M. Martinis, Nature Communications **5**, 5184 (2014).

[76] C. Lang, C. Eichler, L. Steffen, J. M. Fink, M. J. Woolley, A. Blais, and A. Wallraff, Nat. Phys. **9**, 345 (2013).

[77] D. Ristè, M. Dukalski, C. A. Watson, G. de Lange, M. J. Tiggelman, Y. M. Blanter, K. W. Lehnert, R. N. Schouten, and L. DiCarlo, Nature (London) **502**, 350 (2013).

[78] Y. Yin, Y. Chen, D. Sank, P. J. J. O'Malley, T. C. White, R. Barends, J. Kelly, E. Lucero, M. Mariantoni, A. Megrant, C. Neill, A. Vainsencher, J. Wenner, A. N. Korotkov, A. N. Cleland, and J. M. Martinis, Phys. Rev. Lett. **110**, 107001 (2013).

[79] A. O. Niskanen, K. Harrabi, F. Yoshihara, Y. Nakamura, S. Lloyd, and J. S. Tsai, Science **316**, 723 (2007).

[80] D. Bozyigit, C. Lang, L. Steffen, J. M. Fink, C. Eichler, M. Baur, R. Bianchetti, P. J. Leek, S. Filipp, M. P. da Silva, A. Blais, and A. Wallraff, Nat. Phys. **7**, 154 (2010).

[81] S. Kumar and D. P. DiVincenzo, Phys. Rev. B **82**, 014512 (2010).

[82] B. R. Johnson, M. D. Reed, A. A. Houck, D. I. Schuster, L. S. Bishop, E. Ginossar, J. M. Gambetta, L. DiCarlo, L. Frunzio, S. M. Girvin, and R. J. Schoelkopf, Nat. Phys. **6**, 663 (2010).

[83] C. Deng, J. M. Gambetta, and A. Lupascu, Phys. Rev. B **82**, 220505 (2010).

[84] M. Mirrahimi, Z. Leghtas, V. V. Albert, S. Touzard, R. J. Schoelkopf, L. Jiang, and M. H. Devoret, New J. Phys. **16**, 045014 (2014).

[85] A. Sarlette, J. M. Raimond, M. Brune, and P. Rouchon, Phys. Rev. Lett. **107**, 010402 (2011).

[86] A. Roy, Z. Leghtas, A. D. Stone, M. Devoret, and M. Mirrahimi, Phys. Rev. A **91**, 013810 (2015).

[87] Z. Leghtas, S. Touzard, I. M. Pop, A. Kou, B. Vlastakis, A. Petrenko, K. M. Sliwa, A. Narla, S. Shankar, M. J. Hatridge, M. Reagor, L. Frunzio, R. J. Schoelkopf, M. Mirrahimi, and M. H. Devoret, arXiv:1412.4633.

[88] M. Atala, M. Aidelsburger, J. T. Barreiro, D. Abanin, T. Kitagawa, E. Demler, and I. Bloch, Nat. Phys. **9**, 795 (2013).

[89] A. Polkovnikov, K. Sengupta, A. Silva, and M. Vengalattore, Rev. Mod. Phys. **83**, 863 (2011).

[90] M. A. Cazalilla, R. Citro, T. Giamarchi, E. Orignac, and M. Rigol, Rev. Mod. Phys. **83**, 1405 (2011).

[91] C. C. Chien, M. Di Ventra, and M. Zwolak, Phys. Rev. A **90**, 023624 (2014).